
GPart: End-to-End Isometric Fine-Tuning via Global Parameter Partitioning

Paolo Mandica^{1,*,\dagger} Michał Brzozowski^{1,*} Zuzanna Dubanowska¹
 Neo Christopher Chung^{1,2}

¹Samsung AI Center, Warsaw, Poland ²University of Warsaw, Poland

*Equal contribution

^{\dagger}Corresponding author: p.mandica@samsung.com

Abstract

Low-rank adaptation (LoRA) has become the dominant paradigm for parameter-efficient fine-tuning (PEFT) of large language models (LLMs). However, its bilinear structure introduces a critical limitation: the mapping from trainable parameters to weight updates is not distance-preserving, distorting the optimization landscape. Methods that project a low-dimensional vector into LoRA’s parameter space, such as Uni-LoRA, improve parameter efficiency, but the subsequent bilinear LoRA map breaks end-to-end isometry, leaving the core distance-preservation problem unresolved. We propose **GPart** (Global Partition fine-tuning), a highly parameter-efficient fine-tuning method which removes the low-rank bottleneck entirely. Our method uses a single isometric partition matrix to map a d -dimensional trainable vector directly into the full weight space of the model. The result is an extremely minimal fine-tuning pipeline: one random projection, end-to-end isometric, with a single clean hyperparameter (d) and storage cost of $d + 1$ values (the trainable vector plus a random seed). GPart builds on the theoretical premise that effective fine-tuning can emerge from random low-dimensional subspaces of the full weight space, without imposing low-rank matrix structure. We empirically demonstrate the superior or comparable performance of GPart to existing PEFT methods on natural language understanding, computer vision tasks, and mathematical reasoning. Overall, GPart achieves state-of-the-art efficiency and performance by removing structural constraints, offering a straightforward and elegant path to PEFT.

1 Introduction

Fine-tuning pretrained models on downstream tasks is effective, but updating all parameters becomes computationally prohibitive as models grow. Parameter-efficient fine-tuning (PEFT) addresses this by restricting updates to a low-dimensional trainable subspace. Among PEFT methods, LoRA [Hu et al., 2022] is the most widely used: for a weight matrix $W \in \mathbb{R}^{m \times n}$, it parameterizes the update as

$$\Delta W = BA, \quad B \in \mathbb{R}^{m \times r}, \quad A \in \mathbb{R}^{r \times n}, \quad (1)$$

so that only $r(m + n)$ parameters are trained per layer.

LoRA is computationally efficient and empirically strong, but its low-rank bilinear parameterization imposes additional structure on the trainable subspace. In particular, the map from trainable parameters (A, B) to the weight update BA is not an isometry, so Euclidean distances in parameter space are not preserved in weight space. As a result, the geometry seen by the optimizer in the trainable coordinates need not align with the geometry of the induced weight updates.

Recent work has pushed PEFT to even smaller trainable parameter budgets. VeRA [Kopiczko et al., 2024] freezes random matrices and trains only scaling vectors. Uni-LoRA [Li et al., 2025] further

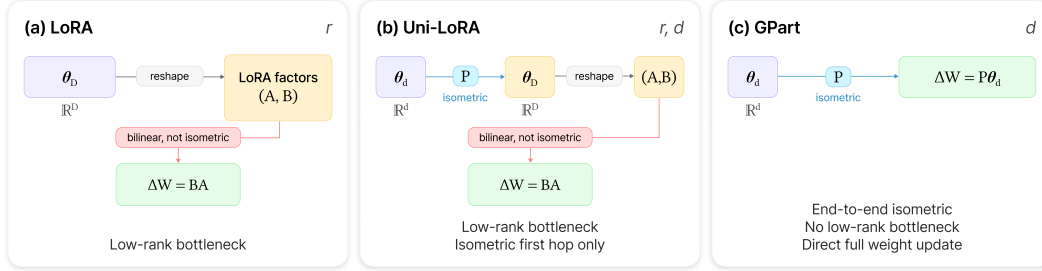


Figure 1: Comparison of PEFT parameterizations. LoRA and Uni-LoRA construct weight updates through the bilinear map $\Delta W = BA$, which breaks end-to-end distance preservation. GPart instead projects the trainable vector directly into full weight space with a seed-generated partition matrix P , yielding a one-step isometric parameterization with d as the only hyperparameter.

compresses the trainable space by optimizing a single d -dimensional vector θ_d , which is mapped into the LoRA parameter space \mathbb{R}^D through a random partition matrix $P \in \mathbb{R}^{D \times d}$ satisfying $P^\top P = I_d$. This projection is isometric, enabling a compact representation in which the trainable state is given by θ_d together with a random seed.

However, in Uni-LoRA the isometry holds only for the projection into LoRA parameter space:

$$\mathbb{R}^d \xrightarrow{P, \text{isometry}} \mathbb{R}^D \xrightarrow{(A,B) \mapsto BA} \mathbb{R}^N. \quad (2)$$

The second stage remains the LoRA bilinear map, so the overall map from θ_d to weight space is not isometric. Thus, although Uni-LoRA removes redundancy within LoRA’s parameterization, it still inherits the low-rank bottleneck and the geometric distortion induced by the map $(A, B) \mapsto BA$.

We propose **GPart** (Global Partition fine-tuning), which removes the intermediate low-rank parameterization entirely. Instead of projecting into LoRA space, GPart maps the trainable vector directly into the full weight space:

$$W = W_0 + P\theta_d, \quad P \in \mathbb{R}^{N \times d}, \quad P^\top P = I_d. \quad (3)$$

This yields a single linear map

$$\mathbb{R}^d \xrightarrow{P, \text{isometry}} \mathbb{R}^N, \quad (4)$$

so the trainable coordinates are connected to the weight update through an end-to-end isometric parameterization of the optimized subspace.

This parameterization also simplifies model selection. In LoRA, the rank r controls both the size and the structure of the low-rank update. In Uni-LoRA, the trainable budget is controlled by d , but r must still be chosen because the method retains the LoRA factorization. GPart removes this extra choice: d , the number of partition groups, is the only hyperparameter controlling subspace size. Figure 1 provides an overview of the three parameterizations.

Conceptually, GPart reconnects PEFT to intrinsic-dimension results. Aghajanyan et al. [2021] showed that strong fine-tuning performance can emerge from optimization in random low-dimensional subspaces of the full parameter space. GPart follows this perspective directly while retaining the storage efficiency emphasized by VeRA and Uni-LoRA.

Our contributions are as follows:

- We introduce GPart, a PEFT method that maps a d -dimensional trainable vector directly into the full weight space via a random partition matrix, eliminating the intermediate low-rank factorization used in LoRA-based approaches.
- We show theoretically that GPart preserves Euclidean geometry within the trainable subspace, whereas the LoRA bilinear map does not.
- We empirically show that GPart is an effective alternative to Uni-LoRA and other PEFT methods across both encoder and decoder settings: at low parameter budgets, it outperforms existing approaches on natural language understanding and computer vision benchmarks while remaining competitive on decoder-only models and mathematical reasoning tasks.

2 Related Work

Low-rank adaptation. LoRA [Hu et al., 2022] parameterizes weight updates as a low-rank product, $\Delta W = BA$, and has become a de facto standard to parameter-efficient fine-tuning (PEFT). A number of follow-up methods modify this parameterization. For example, DoRA [Liu et al., 2024] separates magnitude and direction, while other variants such as AdaLoRA [Zhang et al., 2023] adapt the rank allocation across layers. Despite these differences, these methods retain the low-rank bilinear structure that maps trainable parameters to weight updates through BA .

Hyperefficiency in PEFT. Following the introduction of LoRA, related PEFT methods are introduced to further reduce the number of trainable parameters. BitFit [Ben Zaken et al., 2022] updates only bias parameters, showing that strong adaptation can be achieved with extremely small trainable subsets. VeRA [Kopiczko et al., 2024] freezes random matrices and learns only scaling vectors, enabling compact storage through the learned parameters and a random seed. FourierFT [Gao et al., 2024] reparameterizes weight updates in the frequency domain, learning a small number of Fourier coefficients per layer to reconstruct the full update via the inverse discrete Fourier transform. Uni-LoRA [Li et al., 2025] trains a single low-dimensional vector and projects it into the LoRA parameter space using a random partition matrix. GPart is closest in spirit to VeRA and Uni-LoRA in its use of seed-generated random projections, but differs in that it maps directly into the full weight space rather than into an intermediate LoRA parameterization.

Intrinsic dimensionality and random subspaces. Our work is also closely related to intrinsic-dimension approaches to fine-tuning. Aghajanyan et al. [2021] showed that effective fine-tuning can often be achieved by optimizing within a random low-dimensional subspace of the full parameter space. Their method projects a d -dimensional trainable vector into \mathbb{R}^N using the Fastfood transform [Le et al., 2013], thereby directly parameterizing updates in the ambient weight space. GPart follows the same high-level random-subspace perspective, but uses a sparse partition-based projection instead of a structured dense transform.

Hash-based parameter sharing. GPart is also related to earlier work on parameter sharing through hashing. HashedNet [Chen et al., 2015] compresses neural networks by assigning weights to shared hash buckets, so that multiple weights reuse the same learned parameter. This mechanism is algebraically similar to the partition matrix used in GPart, where each parameter index is assigned to one of d groups. The setting, however, is different: HashedNet was introduced for model compression and training compact models, whereas GPart uses the same type of sharing structure to parameterize fine-tuning updates around a pretrained model.

3 Method

We begin by describing GPart in the vectorized weight space of the pretrained model and comparing it with the LoRA-based factor space; we then formalize the construction of the partition matrix and the resulting forward and backward passes. Figure 2 provides an overview of the full pipeline.

3.1 Vectorized weight space

Consider a pretrained model with L adapted weight matrices $W^{(1)}, W^{(2)}, \dots, W^{(L)}$, possibly of different shapes. We flatten each matrix and concatenate the results into a single parameter vector

$$w_0 = \text{Concat}\left(\text{vec}(W^{(1)}), \text{vec}(W^{(2)}), \dots, \text{vec}(W^{(L)})\right) \in \mathbb{R}^N, \quad (5)$$

where

$$N = \sum_{\ell=1}^L m_\ell n_\ell$$

is the total number of adapted parameters.

For comparison, Uni-LoRA parameterizes updates in the LoRA factor space rather than in \mathbb{R}^N . For each adapted layer ℓ , LoRA introduces factors $B^{(\ell)} \in \mathbb{R}^{m_\ell \times r}$ and $A^{(\ell)} \in \mathbb{R}^{r \times n_\ell}$. Flattening and

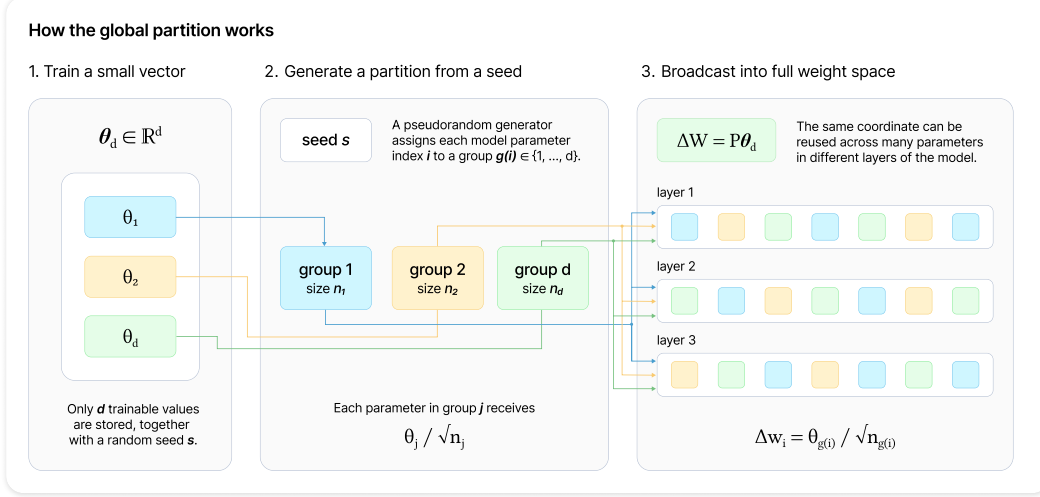


Figure 2: **Overview of GPart.** A d -dimensional trainable vector θ_d is broadcast into the full weight space via a random partition generated from a seed s . Each model parameter w_i is assigned to a group $g(i) \in \{1, \dots, d\}$ and updated as $\Delta w_i = \theta_{g(i)} / \sqrt{n_{g(i)}}$, preserving isometry. The entire fine-tuned model is recovered from only $d + 1$ stored values.

concatenating these variables across layers gives

$$\theta_D = \text{Concat}\left(\text{vec}(B^{(1)}), \text{vec}(A^{(1)}), \dots, \text{vec}(B^{(L)}), \text{vec}(A^{(L)})\right) \in \mathbb{R}^D, \quad (6)$$

with

$$D = \sum_{\ell=1}^L r(m_\ell + n_\ell),$$

typically satisfying $D \ll N$.

Unlike Uni-LoRA, GPart operates directly in the model weight space \mathbb{R}^N . It therefore requires neither low-rank factors nor a bilinear map from factor space back to model space.

3.2 Partition matrix

Let $d \ll N$ denote the dimension of the trainable subspace, where N is the total number of adapted parameters. GPart defines a sparse matrix $P \in \mathbb{R}^{N \times d}$ by first flattening these adapted parameters into a global vector of length N , applying a seed-dependent pseudorandom permutation, and then splitting the permuted sequence into d disjoint groups. This yields a global assignment map

$$g : \{1, \dots, N\} \rightarrow \{1, \dots, d\},$$

such that each parameter belongs to exactly one group and every group is nonempty.

For each group j , define

$$n_j = |\{i : g(i) = j\}|.$$

The matrix P is then given entrywise by

$$P_{ij} = \begin{cases} \frac{1}{\sqrt{n_j}}, & \text{if } g(i) = j, \\ 0, & \text{otherwise.} \end{cases} \quad (7)$$

By construction, each row of P contains exactly one nonzero entry, while distinct columns have disjoint supports. Since every group is nonempty, each column has unit norm, and therefore

$$P^\top P = I_d. \quad (8)$$

Hence, P is an isometric embedding from \mathbb{R}^d into \mathbb{R}^N .

The assignment is global: parameters are grouped across the entire model rather than separately within each layer, and in practice GPart is implemented through the seed-defined assignment $g(\cdot)$ and the group sizes $\{n_j\}_{j=1}^d$, without explicitly materializing P . Figure 2 illustrates both the partition construction and the induced broadcast update.

3.3 Forward and backward passes

Given the pretrained weight vector $w_0 \in \mathbb{R}^N$ and trainable parameters $\theta_d \in \mathbb{R}^d$, GPart defines the adapted weights as

$$w = w_0 + \Delta w, \quad \Delta w = P\theta_d. \quad (9)$$

Equivalently, each parameter i receives the update

$$\Delta w_i = \frac{\theta_{g(i)}}{\sqrt{n_{g(i)}}}. \quad (10)$$

Thus, all parameters assigned to the same group share one trainable value, normalized by the group size. Computing $P\theta_d$ requires only a single pass over the N parameters and no explicit matrix multiplication.

For a loss $\mathcal{L}(w)$, the gradient with respect to θ_d is

$$\nabla_{\theta_d} \mathcal{L} = P^\top \nabla_w \mathcal{L}. \quad (11)$$

In coordinates,

$$(\nabla_{\theta_d} \mathcal{L})_j = \sum_{i: g(i)=j} \frac{(\nabla_w \mathcal{L})_i}{\sqrt{n_j}}. \quad (12)$$

The backward pass therefore reduces to accumulating normalized gradient sums within each group, which again requires $O(N)$ work.

We initialize the trainable vector θ_d at zero. Since GPart is linear in θ_d , this gives $\Delta w = P\theta_d = 0$ at initialization, so optimization starts exactly from the pretrained model w_0 . Unlike bilinear parameterizations such as LoRA, no symmetry-breaking random initialization is required: from Equation (11), the gradient with respect to θ_d is generally nonzero even when $\theta_d = 0$.

3.4 Storage and hyperparameter

The adapted model is fully specified by the seed s , which regenerates the partition, and the trainable vector $\theta_d \in \mathbb{R}^d$, requiring only $d + 1$ stored values. This matches Uni-LoRA while being more storage-efficient than standard LoRA ($O(D)$ parameters) and full fine-tuning ($O(N)$ parameters).

GPart is controlled by a single hyperparameter, the subspace dimension d . Setting $d = 1$ collapses all parameters to one shared scalar, while $d = N$ recovers full fine-tuning; intermediate values interpolate between these extremes. Unlike LoRA-based methods, which require choosing r and, in Uni-LoRA, also d , GPart uses d alone to control the trade-off between parameter efficiency and expressiveness.

4 Theoretical Analysis

We analyze the geometry induced by GPart and contrast it with that of LoRA-based parameterizations. Our central observation is that GPart defines a linear isometric embedding from the trainable space into the full weight space, whereas LoRA-based methods map trainable parameters to weight updates through a bilinear transformation whose local geometry depends on the current parameter values. As a result, GPart preserves the geometry of optimization within its trainable subspace, while LoRA-based parameterizations generally do not.

4.1 End-to-end isometry of GPart

We begin with the basic geometric property of GPart.

Proposition 1 (GPart isometry). *Let $P \in \mathbb{R}^{N \times d}$ be the partition matrix defined in Section 3, satisfying $P^\top P = I_d$. Then for any $\theta, \theta' \in \mathbb{R}^d$,*

$$\|P\theta - P\theta'\|_2 = \|\theta - \theta'\|_2. \quad (13)$$

Proof. By linearity,

$$\|P\theta - P\theta'\|_2^2 = \|P(\theta - \theta')\|_2^2 = (\theta - \theta')^\top P^\top P (\theta - \theta') = (\theta - \theta')^\top (\theta - \theta') = \|\theta - \theta'\|_2^2.$$

Taking square roots gives the result. \square

Proposition 1 shows that GPart preserves Euclidean geometry exactly within the trainable subspace. Equivalently, the map $\theta \mapsto P\theta$ preserves norms, distances, and inner products on \mathbb{R}^d . Thus, optimization in θ -space is exactly optimization over the subspace $\text{image}(P) \subset \mathbb{R}^N$ expressed in orthonormal coordinates.

4.2 LoRA induces a parameter-dependent metric

We now contrast this with the LoRA parameterization. For a single layer, LoRA represents the weight update as

$$\phi(A, B) = BA, \quad B \in \mathbb{R}^{m \times r}, \quad A \in \mathbb{R}^{r \times n}. \quad (14)$$

Unlike GPart, this map is bilinear rather than linear. Its local behavior is therefore governed by a Jacobian that depends on the current values of A and B .

Using $\text{vec}(XYZ) = (Z^\top \otimes X) \text{vec}(Y)$, we obtain

$$\text{vec}(BA) = (I_n \otimes B) \text{vec}(A) \quad \text{and} \quad \text{vec}(BA) = (A^\top \otimes I_m) \text{vec}(B).$$

Hence,

$$\frac{\partial \text{vec}(BA)}{\partial \text{vec}(A)} = I_n \otimes B, \quad \frac{\partial \text{vec}(BA)}{\partial \text{vec}(B)} = A^\top \otimes I_m. \quad (15)$$

These Jacobian blocks depend explicitly on A and B . Consequently, the metric induced on the trainable coordinates by the map $(A, B) \mapsto BA$ varies with the current point in parameter space. In particular, there is no fixed orthonormal coordinate system in (A, B) -space whose Euclidean geometry is preserved by the LoRA map throughout training. Equal-norm perturbations in trainable coordinates can therefore produce different update magnitudes depending on the current values of A and B .

4.3 Connection to intrinsic dimensionality

The motivation for GPart is closely related to the intrinsic-dimensionality view of fine-tuning introduced by Aghajanyan et al. [2021]. That perspective suggests that strong fine-tuning performance can often be recovered by optimizing within a random low-dimensional subspace of the full parameter space.

GPart follows this viewpoint directly by selecting a random d -dimensional subspace of the ambient weight space \mathbb{R}^N and optimizing within that subspace. Because the embedding $P : \mathbb{R}^d \rightarrow \mathbb{R}^N$ is isometric, the restricted optimization problem is represented in orthonormal coordinates without additional distortion introduced by the parameterization.

The key distinction from Uni-LoRA is therefore the location of the random subspace. GPart chooses a subspace directly in full weight space, whereas Uni-LoRA chooses a subspace in LoRA parameter space and then maps it into weight space through a bilinear transformation. The former preserves the geometry of the restricted problem exactly, whereas the latter does not.

5 Experiments

We evaluate GPart across encoder-only and decoder-only models on three benchmark families: natural language understanding, mathematical reasoning, and computer vision. We compare against both non-PEFT baselines—Linear Probing (LP), which updates only the task-specific head, and Full Fine-tuning (FF), which updates all model parameters—and standard PEFT baselines, including LoRA [Hu

et al., 2022], BitFit [Ben Zaken et al., 2022], VeRA [Kopiczko et al., 2024], FourierFT [Gao et al., 2024] and Uni-LoRA [Li et al., 2025]. The reported trainable-parameter counts (# Params) exclude the task-specific head and include only backbone parameters for FF and adapter parameters for PEFT methods. Detailed training hyperparameters for each setup are provided in Appendix E.

5.1 Natural language understanding

We evaluate GPart on GLUE [Wang et al., 2019] using RoBERTa-base and RoBERTa-large [Liu et al., 2019]. In Table 1, we report results on CoLA, SST-2, MRPC, STS-B, QNLI, and RTE, using Matthews correlation for CoLA, Pearson correlation for STS-B, and accuracy for the remaining tasks, following standard practice [Wang et al., 2019, Hu et al., 2022, Li et al., 2025]. For each task, we reserve a portion of each training set as a development set for checkpoint selection, and report the median and standard deviation across three random seeds over the validation set. All models and adapters are fine-tuned by us under this train/dev/val evaluation protocol to ensure a consistent comparison across methods. Full training details are provided in Table 6.

Table 1: GLUE validation results for RoBERTa-base and RoBERTa-large. Bold indicates the best result among PEFT methods, underlined entries indicate the second-best result, and highlighted entries mark cases where GPart outperforms Uni-LoRA.

Model	Method	# Params	CoLA	SST-2	MRPC	STS-B	QNLI	RTE	Avg.
RoBERTa-Base	LP	0	43.1 \pm 2.6	84.3 \pm 0.5	72.5 \pm 0.5	66.3 \pm 0.5	70.6 \pm 0.1	59.2 \pm 1.2	66.0
	FF	124M	60.6 \pm 2.1	94.3 \pm 0.5	87.8 \pm 0.9	90.5 \pm 0.1	92.2 \pm 0.3	77.3 \pm 0.5	83.8
	LoRA ($r=8$)	294K	60.5 \pm 1.2	94.0 \pm 0.6	87.8 \pm 0.5	90.8 \pm 0.2	92.8 \pm 0.1	75.4 \pm 1.0	<u>83.5</u>
	BitFit	102K	58.5 \pm 1.0	93.6 \pm 0.2	<u>88.0</u> \pm 1.2	90.2 \pm 0.0	91.8 \pm 0.1	78.7 \pm 6.1	<u>83.5</u>
	VeRA ($r=1024$)	43K	60.8 \pm 0.7	94.0 \pm 0.2	87.5 \pm 0.2	90.2 \pm 0.1	91.9 \pm 0.0	76.2 \pm 2.9	83.4
	Uni-LoRA	23K	58.1 \pm 0.0	<u>94.2</u> \pm 0.5	86.5 \pm 0.8	90.3 \pm 0.1	<u>92.0</u> \pm 0.3	76.9 \pm 1.7	83.0
GPart (<i>Ours</i>)	23K	<u>60.6</u> \pm 1.9	94.3 \pm 0.5	88.5 \pm 0.6	<u>90.4</u> \pm 0.1	91.1 \pm 0.1	<u>77.3</u> \pm 0.0	83.7	
RoBERTa-Large	LP	0	44.9 \pm 1.1	86.8 \pm 0.6	72.3 \pm 1.1	58.8 \pm 0.3	66.8 \pm 0.7	58.8 \pm 0.6	64.7
	FF	355M	66.3 \pm 0.5	95.8 \pm 0.3	89.5 \pm 0.2	92.0 \pm 0.4	94.6 \pm 0.2	83.4 \pm 1.2	86.9
	LoRA ($r=8$)	786K	65.3 \pm 1.6	<u>95.6</u> \pm 0.1	<u>88.0</u> \pm 0.6	91.3 \pm 0.2	94.8 \pm 0.2	<u>85.4</u> \pm 0.2	86.7
	BitFit	271K	65.4 \pm 0.6	95.9 \pm 0.2	87.8 \pm 1.2	89.9 \pm 0.4	94.0 \pm 0.2	82.3 \pm 12.5	85.9
	VeRA ($r=256$)	61K	59.1 \pm 3.6	95.9 \pm 0.2	87.8 \pm 0.5	91.0 \pm 0.2	<u>94.1</u> \pm 0.5	87.2 \pm 0.9	85.8
	Uni-LoRA	23K	65.0 \pm 7.3	95.4 \pm 0.1	88.7 \pm 0.5	<u>91.5</u> \pm 0.4	92.9 \pm 1.0	81.8 \pm 3.1	85.9
GPart (<i>Ours</i>)	23K	64.2 \pm 0.1	95.4 \pm 0.2	87.2 \pm 0.8	91.7 \pm 0.2	94.0 \pm 0.2	85.2 \pm 0.9	<u>86.3</u>	

We compare against LP, FF, BitFit, LoRA, VeRA, and Uni-LoRA. GPart and Uni-LoRA are matched exactly by subspace dimension d ; LoRA and VeRA are reported at the closest achievable budget according to their original hyper-parameterizations.

GPart performs strongly at very small parameter budgets. On RoBERTa-base, it achieves the best average among all parameter-efficient methods, outperforming not only Uni-LoRA under the matched budget but also LoRA and VeRA configurations that use substantially more trainable parameters. On RoBERTa-large, GPart again improves over Uni-LoRA on average, though the margin is smaller and some individual tasks favor alternative baselines.

5.2 Mathematical reasoning

We evaluate GPart on mathematical reasoning using a diverse set of pretrained decoder-only, non-reasoning models spanning multiple scales and architectures: Qwen-2.5-0.5B, Qwen2.5-3B, and Qwen-2.5-7B [Yang et al., 2024], Gemma-7B [Gemma Team et al., 2024], and Llama-3.1-8B [Grattafiori et al., 2024]. Following the MetaMath setup [Yu et al., 2023], we fine-tune on MetaMathQA and evaluate on GSM8K [Cobbe et al., 2021] and MATH [Hendrycks et al., 2021], reporting exact-match accuracy on the final answer. We focus on comparison against Uni-LoRA under exactly matched trainable parameter budgets.

The results in Table 2 show that GPart remains competitive with Uni-LoRA on both benchmarks across the full set of architectures. Averaged over models, it slightly outperforms Uni-LoRA, increasing mean accuracy from 69.26 to 69.66 on GSM8K and from 31.56 to 32.03 on MATH. Overall, these results indicate that removing the low-rank bottleneck does not harm decoder-only adaptation, although the gains are less consistent than in the encoder-only and vision settings. Taken together, the average results reinforce that GPart is a competitive alternative to Uni-LoRA under matched parameter budgets.

Table 2: Mathematical reasoning results after fine-tuning on MetaMathQA and evaluating on GSM8K and MATH. We report test accuracy. Bold indicates the best result within each model.

Model	Adapter	# Params	GSM8K	MATH
Qwen-2.5-0.5B	Uni-LoRA	131K	46.02	20.94
	GPart (<i>Ours</i>)	131K	46.70	21.16
Llama-3.1-8B	Uni-LoRA	524K	68.16	22.90
	GPart (<i>Ours</i>)	524K	69.45	22.36
Gemma-7B	Uni-LoRA	524K	72.25	25.76
	GPart (<i>Ours</i>)	524K	71.42	24.80
Qwen-2.5-3B	Uni-LoRA	524K	78.24	40.98
	GPart (<i>Ours</i>)	524K	79.30	41.40
Qwen-2.5-7B	Uni-LoRA	524K	81.65	47.20
	GPart (<i>Ours</i>)	524K	81.43	50.42
Average	Uni-LoRA	//	69.26	31.56
	GPart (<i>Ours</i>)	//	69.66	32.03

Table 3: Comparison with baseline approaches across eight computer vision datasets using ViT-Base and ViT-Large backbones. Results for LP, FF, FourierFT, and Uni-LoRA are taken from the Uni-LoRA paper [Li et al., 2025]. Bold indicates the best result among PEFT methods, and highlighted entries mark cases where GPart outperforms Uni-LoRA.

Model	Method	# Params	OxfordPets	StanfordCars	CIFAR10	DTD	EuroSAT	FGVC	RESISC45	CIFAR100	Avg.
ViT-Base	LP	0	90.28 \pm 0.43	25.76 \pm 0.28	96.41 \pm 0.02	69.77 \pm 0.67	88.72 \pm 0.13	17.44 \pm 0.43	74.22 \pm 0.10	84.28 \pm 0.11	68.36
	FF	85.8M	93.14 \pm 0.40	79.78 \pm 1.15	98.92 \pm 0.05	77.68 \pm 1.21	99.05 \pm 0.09	54.84 \pm 1.23	96.13 \pm 0.13	92.38 \pm 0.13	86.49
	FourierFT	72K	93.21 \pm 0.26	46.11 \pm 0.24	98.58 \pm 0.07	75.09 \pm 0.37	98.29 \pm 0.04	27.51 \pm 0.64	91.97 \pm 0.31	91.20 \pm 0.14	77.75
	FourierFT	239K	93.05 \pm 0.34	56.36 \pm 0.66	98.69 \pm 0.06	77.30 \pm 0.61	98.78 \pm 0.11	32.44 \pm 0.99	94.26 \pm 0.20	91.45 \pm 0.18	80.29
	Uni-LoRA	72K	94.00 \pm 0.13	76.06 \pm 0.23	98.77 \pm 0.03	76.99 \pm 0.96	98.86 \pm 0.10	50.36 \pm 0.63	94.08 \pm 0.19	92.10 \pm 0.25	85.15
	GPart (<i>Ours</i>)	72K	93.85 \pm 0.14	77.12 \pm 0.13	98.77 \pm 0.05	77.52 \pm 1.59	99.00 \pm 0.10	56.84 \pm 0.17	94.29 \pm 0.22	92.11 \pm 0.11	86.19
ViT-Large	LP	0	91.11 \pm 0.30	37.91 \pm 0.27	97.78 \pm 0.04	73.33 \pm 0.26	92.64 \pm 0.08	24.62 \pm 0.24	82.02 \pm 0.11	84.28 \pm 0.11	72.96
	FF	303.3M	94.43 \pm 0.56	88.90 \pm 0.26	99.15 \pm 0.04	81.79 \pm 1.01	99.04 \pm 0.08	68.25 \pm 1.63	96.43 \pm 0.07	93.58 \pm 0.19	90.20
	FourierFT	144K	94.46 \pm 0.28	69.56 \pm 0.30	99.10 \pm 0.04	80.83 \pm 0.43	98.65 \pm 0.09	39.92 \pm 0.68	93.86 \pm 0.14	93.31 \pm 0.09	83.71
	FourierFT	480K	94.84 \pm 0.05	79.14 \pm 0.67	99.08 \pm 0.05	81.88 \pm 0.50	98.66 \pm 0.03	51.28 \pm 0.66	95.20 \pm 0.07	93.37 \pm 0.11	86.68
	Uni-LoRA	144K	94.65 \pm 0.23	83.16 \pm 0.62	98.77 \pm 0.03	81.35 \pm 0.48	98.89 \pm 0.07	58.89 \pm 0.62	95.24 \pm 0.12	93.08 \pm 0.11	88.00
	GPart (<i>Ours</i>)	144K	93.86 \pm 0.36	85.20 \pm 0.29	99.11 \pm 0.03	78.74 \pm 1.08	99.08 \pm 0.02	61.48 \pm 0.41	95.09 \pm 0.19	92.59 \pm 0.15	88.14

5.3 Computer vision tasks

Finally, we evaluate GPart on eight computer vision benchmarks to test whether the method transfers beyond language tasks. We follow the protocol used in FourierFT [Gao et al., 2024] and later adopted in Uni-LoRA [Li et al., 2025], using ViT-Base and ViT-Large [Dosovitskiy et al., 2021] pretrained backbones. To align with prior work, we use matched adapter budgets of 72K trainable parameters for ViT-Base and 144K for ViT-Large. For each experiment we report mean \pm standard deviation over five random seeds. Additional implementation details can be found in Table 8. Table 3 shows that GPart achieves the strongest average among the parameter-efficient methods on both ViT-Base and ViT-Large, improving over Uni-LoRA and approaching the performance of full fine-tuning.

5.4 Additional experiments

We complement the main benchmark results with two experiments examining key design choices in GPart: the sensitivity to the subspace dimension d and the geometry of the induced optimization landscape.

5.4.1 Effect of subspace dimension d

We analyze the sensitivity of GPart to the subspace dimension d by fine-tuning RoBERTa-Large on SST-2 while varying d and keeping all other hyperparameters fixed. As shown in Figure 3, performance increases rapidly as d grows from very small values, then plateaus in the mid-range before slightly declining at large d , consistent with mild overfitting as the parameter budget increases. Practically, d serves as a continuous knob that trades parameter efficiency for model capacity.

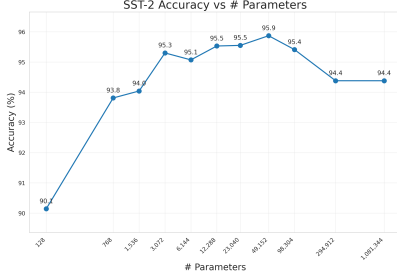


Figure 3: Accuracy on SST-2 with RoBERTa-Large as a function of the subspace dimension d .

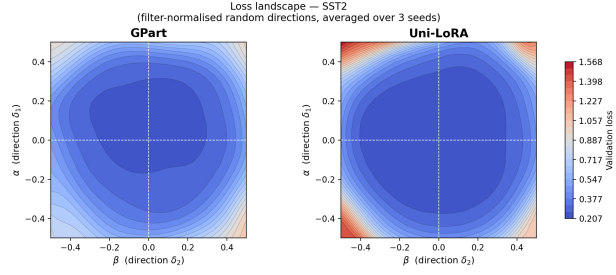


Figure 4: Loss landscape around the converged solution for GPart (left) and Uni-LoRA (right) on SST-2 with RoBERTa-Large and 23K trainable parameters, averaged over three random direction seeds [Li et al., 2018].

5.4.2 Loss landscape geometry

To complement the theoretical analysis of Section 4, we visualize the optimization geometry of GPart and Uni-LoRA using the filter-normalized random-direction method of Li et al. [2018]. For each method, we evaluate the validation loss on a 30×30 grid of perturbations $\theta^* + \alpha\delta_1 + \beta\delta_2$, with $\alpha, \beta \in [-0.5, 0.5]$, where $\delta_1, \delta_2 \in \mathbb{R}^d$ are random directions normalized to have the same ℓ_2 norm as θ^* . Perturbations are confined to the adapter subspace and averaged over three direction seeds.

Figure 4 shows the resulting surfaces on SST-2 with RoBERTa-Large at $d = 23040$. GPart yields a smooth, well-centered basin with gradually rising contours in all directions, consistent with its isometric parameterization preserving Euclidean structure uniformly across the trainable subspace. Uni-LoRA, by contrast, develops sharp high-loss regions in opposing corners, a signature of the bilinear reconstruction step $(A, B) \mapsto BA$: equal steps in θ_d -space can produce direction-dependent weight-space updates, causing the loss to rise steeply along some directions while remaining flat along others. This asymmetry is stable across all three seeds, suggesting that it reflects a structural property of the parameterization rather than a sampling artifact.

6 Limitations

While our empirical evaluation is broad and diverse across encoder-only language models, vision encoders, and decoder-only LLMs, in the future works, we would apply GPart to larger LMs and multimodal LMs. Our decoder-only experiments are limited to a relatively narrow set of models and reasoning benchmarks, so the extent to which the observed trends generalize to broader instruction-following or long-context settings remains unclear. Regarding broader impacts, this work is a methodology-focused contribution to PEFT and does not introduce new application-specific capabilities. We therefore do not identify significant additional societal impacts beyond those of the underlying pretrained models.

7 Conclusion

We introduced GPart, a parameter-efficient fine-tuning method that maps a low-dimensional trainable vector directly into the full model weight space through a random partition matrix. By removing the intermediate low-rank parameterization used by LoRA and its variants, GPart yields an end-to-end isometric parameterization of the optimized subspace while retaining a single hyperparameter, d , to control the trainable budget. Across natural language understanding, mathematical reasoning, and computer vision benchmarks, GPart outperforms or is comparable to existing PEFT methods, while conceptually and practically straightforward to implement. Broadly, these results suggest that effective PEFT does not require a low-rank bottleneck, and that direct random subspace parameterizations constitute a promising alternative from both empirical and theoretical perspectives.

Acknowledgments and Disclosure of Funding

We thank Paweł Olszowiec, Maciej Żelaszczyk, and the members of the Agentic Reasoning Lab at Samsung AI Center Warsaw for insightful discussions and feedback that helped shape this work. We are also grateful to Iлона Harhasevich for her assistance in designing the figures presented in this paper.

References

- Armen Aghajanyan, Sonal Gupta, and Luke Zettlemoyer. Intrinsic dimensionality explains the effectiveness of language model fine-tuning. In Chengqing Zong, Fei Xia, Wenjie Li, and Roberto Navigli, editors, *Proceedings of the 59th Annual Meeting of the Association for Computational Linguistics and the 11th International Joint Conference on Natural Language Processing (Volume 1: Long Papers)*, pages 7319–7328, Online, August 2021. Association for Computational Linguistics. doi: 10.18653/v1/2021.acl-long.568. URL <https://aclanthology.org/2021.acl-long.568/>.
- Elad Ben Zaken, Yoav Goldberg, and Shauli Ravfogel. BitFit: Simple parameter-efficient fine-tuning for transformer-based masked language-models. In Smaranda Muresan, Preslav Nakov, and Aline Villavicencio, editors, *Proceedings of the 60th Annual Meeting of the Association for Computational Linguistics (Volume 2: Short Papers)*, pages 1–9, Dublin, Ireland, May 2022. Association for Computational Linguistics. doi: 10.18653/v1/2022.acl-short.1. URL <https://aclanthology.org/2022.acl-short.1/>.
- Wenlin Chen, James T. Wilson, Stephen Tyree, Kilian Q. Weinberger, and Yixin Chen. Compressing neural networks with the hashing trick. In *International Conference on Machine Learning (ICML)*, 2015. arXiv:1504.04788.
- Karl Cobbe, Vineet Kosaraju, Mohammad Bavarian, Mark Chen, Heewoo Jun, Lukasz Kaiser, Matthias Plappert, Jerry Tworek, Jacob Hilton, Reiichiro Nakano, Christopher Hesse, and John Schulman. Training verifiers to solve math word problems. *arXiv preprint arXiv:2110.14168*, 2021.
- Alexey Dosovitskiy, Lucas Beyer, Alexander Kolesnikov, Dirk Weissenborn, Xiaohua Zhai, Thomas Unterthiner, Mostafa Dehghani, Matthias Minderer, Georg Heigold, Sylvain Gelly, Jakob Uszkoreit, and Neil Houlsby. An image is worth 16x16 words: Transformers for image recognition at scale. *ICLR*, 2021.
- William Fleshman and Benjamin Van Durme. SpectR: Dynamically composing LM experts with spectral routing. *arXiv preprint arXiv:2504.03454*, 2025.
- Ziqi Gao, Qichao Wang, Aochuan Chen, Zijing Liu, Bingzhe Wu, Liang Chen, and Jia Li. Parameter-efficient fine-tuning with discrete fourier transform. In *Forty-first International Conference on Machine Learning, ICML 2024, Vienna, Austria, July 21-27, 2024*, 2024.
- Thomas Mesnard Gemma Team, Cassidy Hardin, Robert Dadashi, Surya Bhupatiraju, Laurent Sifre, Morgane Rivière, Mihir Sanjay Kale, Juliette Love, Pouya Tafti, Léonard Hussenot, and et al. Gemma. 2024. doi: 10.34740/KAGGLE/M/3301. URL <https://www.kaggle.com/m/3301>.
- Aaron Grattafiori, Abhimanyu Dubey, Abhinav Jauhri, Abhinav Pandey, Abhishek Kadian, Ahmad Al-Dahle, Aiesha Letman, Akhil Mathur, Alan Schelten, Alex Vaughan, et al. The llama 3 herd of models. *arXiv preprint arXiv:2407.21783*, 2024.
- Ziyi Han, Huanyu Wang, Zeyu Zhang, Xiangxiang Dai, Xutong Liu, and John C.S. Lui. HiLoRA: Adaptive hierarchical LoRA routing for training-free domain generalization. *arXiv preprint arXiv:2510.12266*, 2025.
- Soufiane Hayou, Nikhil Ghosh, and Bin Yu. LoRA+: Efficient low rank adaptation of large models. In *Proceedings of the 41st International Conference on Machine Learning*, volume 235 of *Proceedings of Machine Learning Research*, pages 17783–17806. PMLR, 2024.

- Dan Hendrycks, Collin Burns, Saurav Kadavath, Akul Arora, Steven Basart, Eric Tang, Dawn Song, and Jacob Steinhardt. Measuring mathematical problem solving with the math dataset. *NeurIPS*, 2021.
- Edward J Hu, yelong shen, Phillip Wallis, Zeyuan Allen-Zhu, Yuanzhi Li, Shean Wang, Lu Wang, and Weizhu Chen. LoRA: Low-rank adaptation of large language models. In *International Conference on Learning Representations*, 2022. URL <https://openreview.net/forum?id=nZeVKeeFYf9>.
- Damjan Kalajdziewski. A rank stabilization scaling factor for fine-tuning with LoRA. *arXiv preprint arXiv:2312.03732*, 2023.
- Dawid Jan Kopiczko, Tijmen Blankevoort, and Yuki M Asano. VeRA: Vector-based random matrix adaptation. In *The Twelfth International Conference on Learning Representations*, 2024. URL <https://openreview.net/forum?id=NjNfLdxr3A>.
- Quoc Le, Tamás Sarlós, and Alex Smola. Fastfood — approximating kernel expansions in loglinear time. In *International Conference on Machine Learning (ICML)*, 2013.
- Yu-Ang Lee, Ching-Yun Ko, Pin-Yu Chen, and Mi-Yen Yeh. Learning rate matters: Vanilla lora may suffice for llm fine-tuning, 2026. URL <https://arxiv.org/abs/2602.04998>.
- Hao Li, Zheng Xu, Gavin Taylor, Christoph Studer, and Tom Goldstein. Visualizing the loss landscape of neural nets. In *Neural Information Processing Systems*, 2018.
- Kaiyang Li, Shaobo Han, Qing Su, Wei Li, Zhipeng Cai, and Shihao Ji. Uni-LoRA: One vector is all you need. In *The Thirty-ninth Annual Conference on Neural Information Processing Systems*, 2025. URL <https://openreview.net/forum?id=hzBqQZK2iV>.
- Yixiao Li, Yifan Yu, Chen Liang, Pengcheng He, Nikos Karampatziakis, Weizhu Chen, and Tuo Zhao. LoftQ: LoRA-fine-tuning-aware quantization for large language models. *arXiv preprint arXiv:2310.08659*, 2023.
- Shih-Yang Liu, Chien-Yi Wang, Hongxu Yin, Pavlo Molchanov, Yu-Chiang Frank Wang, Kwang-Ting Cheng, and Min-Hung Chen. DoRA: weight-decomposed low-rank adaptation. In *Proceedings of the 41st International Conference on Machine Learning, ICML'24*. JMLR.org, 2024.
- Yinhan Liu, Myle Ott, Naman Goyal, Jingfei Du, Mandar Joshi, Danqi Chen, Omer Levy, Mike Lewis, Luke Zettlemoyer, and Veselin Stoyanov. RoBERTa: A robustly optimized BERT pretraining approach, 2019. URL <https://arxiv.org/abs/1907.11692>.
- Fanxu Meng, Zhaohui Wang, and Muhan Zhang. PiSSA: Principal singular values and singular vectors adaptation of large language models. In *Advances in Neural Information Processing Systems*, 2024. arXiv:2404.02948.
- Oleksiy Ostapenko, Massimo Caccia, Eugene Belilovsky, Laurent Charlin, Joelle Pineau, and Irina Rish. Towards modular LLMs by building and reusing a library of LoRAs. In *Proceedings of the 41st International Conference on Machine Learning*, volume 235 of *Proceedings of Machine Learning Research*. PMLR, 2024.
- Alex Wang, Amanpreet Singh, Julian Michael, Felix Hill, Omer Levy, and Samuel R. Bowman. GLUE: A multi-task benchmark and analysis platform for natural language understanding. In *International Conference on Learning Representations*, 2019. URL <https://openreview.net/forum?id=rJ4km2R5t7>.
- An Yang, Baosong Yang, Beichen Zhang, Binyuan Hui, Bo Zheng, Bowen Yu, Chengyuan Li, Dayiheng Liu, Fei Huang, Haoran Wei, Huan Lin, Jian Yang, Jianhong Tu, Jianwei Zhang, Jianxin Yang, Jiayi Yang, Jingren Zhou, Junyang Lin, Kai Dang, Keming Lu, Keqin Bao, Kexin Yang, Le Yu, Mei Li, Mingfeng Xue, Pei Zhang, Qin Zhu, Rui Men, Runji Lin, Tianhao Li, Tingyu Xia, Xingzhang Ren, Xuancheng Ren, Yang Fan, Yang Su, Yichang Zhang, Yu Wan, Yuqiong Liu, Zeyu Cui, Zhenru Zhang, and Zihan Qiu. Qwen2.5 technical report. *arXiv preprint arXiv:2412.15115*, 2024.

Longhui Yu, Weisen Jiang, Han Shi, Jincheng Yu, Zhengying Liu, Yu Zhang, James T Kwok, Zhenguo Li, Adrian Weller, and Weiyang Liu. Metamath: Bootstrap your own mathematical questions for large language models. *arXiv preprint arXiv:2309.12284*, 2023.

Qingru Zhang, Minshuo Chen, Alexander Bukharin, Pengcheng He, Yu Cheng, Weizhu Chen, and Tuo Zhao. Adaptive budget allocation for parameter-efficient fine-tuning. In *The Eleventh International Conference on Learning Representations*, 2023. URL <https://openreview.net/forum?id=1q62uWRJjiY>.

Ziyu Zhao, Tao Shen, Didi Zhu, Zexi Li, Jing Su, Xuwu Wang, Kun Kuang, and Fei Wu. Merging LoRAs like playing LEGO: Pushing the modularity of LoRA to extremes through rank-wise clustering. In *International Conference on Learning Representations*, 2025.

A Formal Analysis of GPart’s Isometric Structure

A.1 Partition matrix construction

We provide a self-contained construction of the partition matrix and proof of its isometry property.

Definition 1 (Partition matrix). *Given N parameters, d groups, and a random assignment function $g : \{1, \dots, N\} \rightarrow \{1, \dots, d\}$, the partition matrix $P \in \mathbb{R}^{N \times d}$ is defined by:*

$$P_{ij} = \begin{cases} 1/\sqrt{n_j} & \text{if } g(i) = j, \\ 0 & \text{otherwise,} \end{cases} \quad (16)$$

where $n_j = |\{i : g(i) = j\}|$.

Proposition 2. $P^\top P = I_d$.

Proof. $(P^\top P)_{jk} = \sum_{i=1}^N P_{ij} P_{ik}$. If $j \neq k$, the supports of columns j and k are disjoint (each row has a single non-zero entry), so the sum is 0. If $j = k$, the sum is $\sum_{i:g(i)=j} (1/\sqrt{n_j})^2 = n_j \cdot (1/n_j) = 1$. \square

A.2 Gradient identity

Proposition 3. *For any loss function $\mathcal{L}(w)$ with $w = w_0 + P\theta_d$:*

$$\nabla_{\theta_d} \mathcal{L} = P^\top \nabla_w \mathcal{L}. \quad (17)$$

Moreover, $\|\nabla_{\theta_d} \mathcal{L}\|_2 \leq \|\nabla_w \mathcal{L}\|_2$, with equality when $\nabla_w \mathcal{L}$ lies entirely in the image of P .

Proof. The first identity follows from the chain rule. For the norm bound: $\|\nabla_{\theta_d} \mathcal{L}\|^2 = \|P^\top \nabla_w \mathcal{L}\|^2 = (\nabla_w \mathcal{L})^\top P P^\top (\nabla_w \mathcal{L})$. Since $P P^\top$ is an orthogonal projection onto $\text{image}(P)$, its eigenvalues are 0 and 1, giving the inequality. \square

A.3 Weight decay and regularization

End-to-end isometry also gives GPart a simple interpretation under L2 regularization. If weight decay is applied to θ_d , then

$$\lambda \|\theta_d\|_2^2 = \lambda \|P\theta_d\|_2^2 = \lambda \|\Delta w\|_2^2, \quad (18)$$

where $\Delta w = P\theta_d = w - w_0$. Thus, weight decay on the trainable parameters is exactly weight decay on the induced perturbation in full weight space.

For LoRA, regularization is typically applied to the factors A and B , yielding the penalty

$$\lambda (\|A\|_F^2 + \|B\|_F^2).$$

This does not directly equal the squared norm of the induced weight perturbation $\Delta W = BA$. Instead, by submultiplicativity of the Frobenius norm and the arithmetic–geometric mean inequality,

$$\|\Delta W\|_F = \|BA\|_F \leq \|B\|_F \|A\|_F \leq \frac{1}{2} (\|A\|_F^2 + \|B\|_F^2). \quad (19)$$

Thus, regularization in LoRA controls only an upper bound on the norm of the resulting weight update, rather than the norm itself.

Remark 1. *For Uni-LoRA, applying weight decay to the trainable vector yields an exact norm interpretation in the intermediate LoRA parameter space, since the projection into that space is isometric. However, after the subsequent bilinear map into weight space, the same mismatch as in LoRA remains.*

B The Cost of Breaking Isometry

We study the role of the $1/\sqrt{n_j}$ normalization in GPart by comparing the standard isometric construction with a non-isometric variant in which the normalization is removed. This comparison isolates whether end-to-end isometry is merely a geometric convenience or whether it has a measurable effect on optimization and downstream performance.

B.1 Setup

We compare two variants of GPart that differ only in the column normalization of P :

- **GPart (isometric):** $P_{ij} = 1/\sqrt{n_j}$ if $g(i) = j$, so $P^\top P = I_d$.
- **GPart (non-isometric):** $P_{ij} = 1$ if $g(i) = j$, so $P^\top P = \text{diag}(n_1, \dots, n_d)$.

All other aspects of the method are identical.

B.2 Weight decay miscalibration

The performance gap between the two variants can be understood as a direct consequence of Equation (18). In the isometric case, we have

$$\|\Delta w\|_2^2 = \|P_{\text{iso}}\theta_d\|_2^2 = \|\theta_d\|_2^2,$$

so AdamW weight decay on θ_d with coefficient λ corresponds exactly to L_2 regularization on the induced weight perturbation.

In the non-isometric case, the perturbation associated with group j has magnitude $\sqrt{n_j}\theta_j$, so

$$\|\Delta w\|_2^2 = \sum_j n_j \theta_j^2.$$

AdamW still applies decay directly to θ_j , so the decay acts at scale $\|\theta_d\|_2^2$, while the actual weight perturbation lives at scale $\sum_j n_j \theta_j^2$. Since $n_j \approx N/d$ under a roughly balanced random partition, the regularization is miscalibrated by a factor of approximately N/d . For typical settings such as $N \approx 10^8$ and $d \approx 10^4$, this factor is on the order of 10^4 .

This mismatch is not corrected by Adam’s gradient normalization. Equivalently, the non-isometric parameterization behaves like the isometric variant with the induced weight perturbation scaled up by $\sqrt{n_j}$ while the corresponding regularization strength is scaled down by n_j . In practice, this yields severe under-regularization in weight space.

B.3 Empirical effect of non-isometric P

To test whether this theoretical mismatch has practical consequences, we compare GPart against the non-isometric variant on GLUE using RoBERTa-base and RoBERTa-large at a matched budget of 23K trainable parameters. For fairness, we independently tuned the optimization hyperparameters of the non-isometric variant so that any performance difference in performance cannot be attributed to a mismatched optimization scale. The results are reported in Table 4.

Table 4: Isometric vs. non-isometric GPart on GLUE.

Model	Method	# Params	CoLA	SST-2	MRPC	STS-B	QNLI	RTE	Avg
Base	GPart Non-Iso	23K	44.7 \pm 3.4	93.5 \pm 0.5	87.5 \pm 0.9	90.3 \pm 0.2	91.2 \pm 0.1	77.3 \pm 2.8	80.7
	GPart	23K	60.6 \pm 1.9	94.3 \pm 0.5	88.5 \pm 0.6	90.4 \pm 0.1	91.1 \pm 0.1	77.3 \pm 0.0	83.7
Large	GPart Non-Iso	23K	60.1 \pm 0.6	95.4 \pm 0.3	89.0 \pm 1.6	89.9 \pm 2.3	93.8 \pm 0.1	80.5 \pm 2.2	84.8
	GPart	23K	64.2 \pm 0.1	95.4 \pm 0.2	87.2 \pm 0.8	91.7 \pm 0.2	94.0 \pm 0.2	85.2 \pm 0.9	86.3

Across both RoBERTa-base and RoBERTa-large, the isometric variant achieves a higher average score than the non-isometric variant. The gap is especially pronounced on CoLA for the base model (60.6 vs. 44.7) and on RTE for the large model (85.2 vs. 80.5), indicating that the normalization affects not only average performance but also stability on more sensitive tasks.

These results are consistent with the analysis above. Removing the $1/\sqrt{n_j}$ factor does not merely alter the parameterization algebraically; it changes the relationship between parameter-space regularization and the actual magnitude of the induced weight update. The empirical degradation in Table 4 therefore supports the view that the isometric normalization is a practically important part of GPart rather than a cosmetic design choice.

C Algorithm

Algorithm 1 GPart: Global Partition Fine-Tuning

Require: Pretrained parameters $w_0 \in \mathbb{R}^N$, training set \mathcal{D} , subspace dimension d , seed s , optimizer Opt, initialization $\epsilon > 0$

- 1: Generate a fixed partition map $g : \{1, \dots, N\} \rightarrow \{1, \dots, d\}$ from seed s
- 2: Compute group sizes $n_j = |\{i : g(i) = j\}|$ for $j = 1, \dots, d$
- 3: Initialize $\theta_d = 0$
- 4: Implement P implicitly using only $g(\cdot)$ and $\{n_j\}_{j=1}^d$
- 5: **for** each minibatch $\mathcal{B} \subset \mathcal{D}$ **do**
- 6: Form Δw implicitly using $(\Delta w)_i \leftarrow (\theta_d)_{g(i)} / \sqrt{n_{g(i)}}$ for all i
- 7: Set adapted parameters $w \leftarrow w_0 + \Delta w$
- 8: Compute loss $\mathcal{L}_{\mathcal{B}}(w)$
- 9: Compute $\nabla_{\theta_d} \mathcal{L}_{\mathcal{B}}$ from $\nabla_w \mathcal{L}_{\mathcal{B}}$
- 10: Update $\theta_d \leftarrow \text{Opt}(\theta_d, \nabla_{\theta_d} \mathcal{L}_{\mathcal{B}})$
- 11: **end for**
- 12: **return** s, θ_d

D Comparison of Parameter Counts

Table 5 summarizes the number of trainable parameters introduced by each method, both per adapted layer and globally. Full fine-tuning scales with the total model size N , while LoRA introduces $r(m+n)$ parameters per layer, giving a global count $D = \sum_{\ell} r(m_{\ell} + n_{\ell})$ that grows with depth and layer width. BitFit and VeRA are more frugal, tuning only bias vectors or diagonal scaling factors, but their global counts still accumulate over layers. FourierFT decouples the budget from layer dimensions by fixing d frequencies per layer, yielding a global count of $L \times d$. GPart and Uni-LoRA go one step further: both parameterize the entire adaptation through a *single* global vector $\theta_d \in \mathbb{R}^d$, shared across all L adapted layers, so the parameter count is independent of model depth and layer dimensions. The key distinction between the two methods is therefore not in parameter count — which is identical by construction in our experiments — but in how θ_d is mapped back to weight space.

Table 5: Trainable parameter counts per adapted layer and globally across a model with L adapted layers of dimensions $W_{\ell} \in \mathbb{R}^{m_{\ell} \times n_{\ell}}$, with N denoting total model parameters.

Method	Per layer	Global
Full FT	mn	N
LoRA (rank r)	$r(m+n)$	$\sum_{\ell} r(m_{\ell} + n_{\ell}) = D$
BitFit	m (bias only)	$\sum_{\ell} m_{\ell}$
VeRA	$m+n$ (diag. scaling)	$\sum_{\ell} (m_{\ell} + n_{\ell})$
FourierFT	d	$L \times d$
Uni-LoRA	d (global, shared across all layers)	
GPart	d (global, shared across all layers)	

E Implementation Details

All experiments are run on a single NVIDIA H100 80GB GPU. We use AdamW throughout, with task-specific learning rates for the classification head and the subspace parameters θ_d tuned independently. The partition matrix P is fixed at initialization and applied to the `target_modules` matrices in every transformer block, excluding the task head. Full per-task hyperparameters for natural language understanding, mathematical reasoning, and computer vision are provided in Tables 6, 7, and 8, respectively.

Although GPart operates through a global partition and therefore introduces less regular memory access than low-rank methods, in practice we observe only about a 10% wall-clock slowdown relative to Uni-LoRA. This modest overhead is largely due to an implementation that never explicitly materializes P ; instead, the method stores only the global trainable vector, the parameter-to-group

assignments, and the associated scaling factors, and applies the broadcast update implicitly during the forward and backward passes.

More precisely, each adapted layer gathers the relevant entries of θ_d , rescales them, and reshapes them directly into weight and bias updates before reusing the underlying dense linear operation. In the common single-adapter setting, we further use a custom autograd function that fuses this implicit reconstruction with the linear layer and computes the gradient with respect to θ_d by a direct grouped accumulation, reducing graph overhead and avoiding explicit sparse matrix operations.

Finally, the trainable vector θ_d is stored once at the model level rather than duplicated across layers, while the partition itself is represented through compact index and scale buffers. Together, these choices substantially reduce the practical memory and runtime overhead of operating in the full model weight space.

Table 6: Hyperparameters for GLUE experiments.

Model	Hyperparameter	SST-2	MRPC	CoLA	QNLI	RTE	STS-B
	Optimizer			AdamW			
	Weight Decay			0.1			
	Warmup Ratio			0.06			
	LR Schedule			Linear			
	Init. of θ_d			0			
	LR (θ_d)			5E-3			
	$ \theta_d $			23,040			
	Batch Size Per GPU			32			
	Target Modules			["query", "value"]			
BASE	Epochs	60	30	80	25	160	80
	LR (Head)	5E-4	1E-3	2E-4	1E-3	1E-2	2E-4
	Max Seq. Len.			512			
	Training Time (Total)			154 minutes			
	GPU Memory			19GiB			
LARGE	Epochs	30	30	60	25	120	80
	LR (Head)	2E-4	1E-3	2E-3	1E-3	1E-2	2E-4
	Max Seq. Len.			128			
	Training Time (Total)			66 minutes			
	GPU Memory			15GiB			

Table 7: Hyperparameters for mathematical reasoning experiments.

Hyperparameter	Qwen-2.5-0.5B	Qwen-2.5-3B	Qwen-2.5-7B	Gemma-7B	Llama-3.1-8B
Optimizer			AdamW		
LR Schedule			Cosine		
Batch Size			2		
Accumulation Steps			8		
Warmup Ratio			0.05		
Weight Decay			0.05		
Epochs			2		
Warmup Ratio			0.02		
Target Modules		["q_proj", "k_proj", "v_proj", "o_proj"]			
Init. of θ_d			0		
Max Seq. Len.			2048		
LR (θ_d)			2E-4		
$ \theta_d $	131,072	524,288	524,288	524,288	524,288
Training Time	4h	8h	15h	21h	17h
GPU Memory	19GiB	31GiB	45GiB	66GiB	53GiB

F Why the BA Factorization Is Problematic

The BA parametrization introduced by Hu et al. [2022] is a pragmatic choice: it expresses a rank- r update $\Delta W \in \mathbb{R}^{d_{\text{out}} \times d_{\text{in}}}$ using only $r(d_{\text{in}} + d_{\text{out}})$ parameters, a substantial saving when

Table 8: Hyperparameters for computer vision experiments.

Model	Hyperparameter	OxfordPets	StanfordCars	CIFAR10	DTD	EuroSAT	FGVC	RESISC45	CIFAR100
	Optimizer				AdamW				
	Weight Decay				0.01				
	LR Schedule				Linear				
	Warmup Ratio				0.05				
	Init. of θ_d				0				
	Epochs				20				
	Target Modules				["query", "value"]				
VIT-BASE	LR (Head)	2E-2	3E-3	5E-3	1E-2	1E-2	1E-2	5E-2	5E-3
	LR (θ_d)	1E-2	5E-2	1E-2	1E-2	5E-2	5E-2	8E-2	5E-2
	$ \theta_d $				72,000				
	Batch Size Per GPU				64				
	Training Time	4m	9m	26m	4m	11m	15m	15m	27m
	GPU Memory				5GiB				
VIT-LARGE	LR (Head)	2E-2	3E-3	5E-3	1E-2	1E-2	1E-2	5E-2	5E-3
	LR (θ_d)	1E-2	5E-2	1E-2	1E-2	5E-2	5E-2	8E-2	5E-2
	$ \theta_d $				144,000				
	Batch Size Per GPU				32				
	Training Time	6m	16m	56m	8m	24m	17m	27m	51m
	GPU Memory				8GiB				

$r \ll \min(d_{\text{in}}, d_{\text{out}})$. Despite its empirical success, this factorization introduces a collection of theoretical pathologies that have spawned a large body of follow-up work. We identify the two root causes—a representational non-uniqueness and the asymmetric coupling of the bilinear factors—and show that GPart eliminates both by construction.

F.1 Representational non-uniqueness of LoRA

The bilinear factorization $\Delta W = BA$ is not unique. For any invertible matrix $G \in \mathbb{R}^{r \times r}$, the substitution

$$B \mapsto BG^{-1}, \quad A \mapsto GA$$

leaves ΔW unchanged. The set of all pairs that produce a given ΔW therefore forms an equivalence class

$$[(B, A)] = \{(BG^{-1}, GA) : G \in GL(r)\},$$

and the true object of interest—the linear map ΔW —is an element of the quotient. Any quantity computed from (B, A) that is not invariant under this family of substitutions is a property of the *representation*, not of the underlying adapter.

This non-uniqueness has concrete consequences throughout the LoRA literature:

Routing and merging. Methods that operate directly on the raw (B, A) factorization—such as the rank-one routing of Han et al. [2025] and the clustering-based merging of Zhao et al. [2025]—perform computations on representation-dependent objects. Two adapters that implement identical linear maps ΔW but were trained with different random seeds will in general have different (B, A) pairs, and will therefore be treated as dissimilar by any metric defined on those pairs. The permutation invariance claimed by Zhao et al. [2025] accounts only for the discrete subgroup of signed permutation matrices inside $GL(r)$; the remaining continuous non-uniqueness goes unaddressed.

Scale non-invariance. A special case of this non-uniqueness is the *scale symmetry*: $(B, A) \mapsto (\lambda B, \lambda^{-1}A)$ for any $\lambda \neq 0$. Under this transformation ΔW is unchanged, but any method that computes norms or distances on the columns of B or the rows of A individually will produce different results. This affects, for instance, the token-level routing scores of Han et al. [2025], which score hidden states against columns of B and are therefore arbitrarily sensitive to the optimizer-induced scaling of the factorization.

The SVD as a canonical representative. Ostapenko et al. [2024] and Fleshman and Van Durme [2025] avoid this problem by working with the singular value decomposition $\Delta W = U\Sigma V^\top$ rather than the raw (B, A) pair. When all singular values are distinct—which holds generically for fully trained adapters, since the set of matrices with repeated singular values has measure zero in $\mathbb{R}^{d_{\text{out}} \times d_{\text{in}}}$ —this picks a unique representative from each equivalence class, up to a finite group of

sign flips on singular vector pairs. Since both methods operate post-hoc on trained adapters, this is a principled and largely complete fix within the LoRA framework. GPart eliminates the non-uniqueness entirely by construction: the map $\theta_d \mapsto P\theta_d$ is injective, so every adapter has a unique representation without requiring a post-hoc canonicalization step.

F.2 Pathologies of the bilinear factorization

The factorization $\Delta W = BA$ introduces two coupled matrices whose asymmetric roles generate a cluster of optimization pathologies. Unlike the representational non-uniqueness discussed in Section F.1, these pathologies are not about which ΔW can be expressed, but about how the optimization landscape over (B, A) behaves relative to the underlying objective over ΔW . GPart eliminates both by replacing the bilinear factorization with a single linear map $\theta_d \mapsto P\theta_d$, removing the coupling entirely.

Asymmetric optimization dynamics. The gradient of the loss with respect to B depends on A and vice versa, creating coupled dynamics that are a structural consequence of the bilinear factorization and are not present in full fine-tuning. Hayou et al. [2024] showed that using the same learning rate for A and B is provably suboptimal for large-width networks, and proposed LoRA+ which assigns different learning rates to the two matrices. Kalajdzievski [2023] showed that the standard α/r scaling causes gradient collapse as rank increases, and derived the corrected α/\sqrt{r} scaling. Both issues are absent in GPart by construction: since there is no bilinear factorization, there are no coupled factors A and B to which these pathologies can apply.

Initialization pathology. LoRA initializes $B = 0$ so that $\Delta W = BA = 0$ at the start of training, ensuring the fine-tuned model begins from the pretrained weights. This convention is structurally forced by the bilinear factorization: there is no symmetric way to initialize (B, A) to zero output while keeping both matrices in a generic position. The asymmetry has spawned a line of work proposing alternative initializations, including PiSSA [Meng et al., 2024], which initializes from the top- r singular components of W_0 , and LoftQ [Li et al., 2023], which handles the quantized setting. Recent work suggests that these gains may be largely attributable to the learning rate regimes they induce rather than the initializations themselves [Lee et al., 2026], which is consistent with the view that the initialization literature is patching a symptom rather than the root cause. In GPart, any initialization of θ_d produces a well-defined $\Delta W = P\theta_d$ from step one, and the question of how to initialize the adapter does not interact with the structure of the map itself.

F.3 Summary

Table 9 summarizes the pathologies of the BA factorization discussed above, the fixes proposed in the literature, and whether each is absent in GPart by construction.

Table 9: Pathologies of the LoRA BA factorization and their status in GPart. \checkmark = present; \times = absent by construction. The final column indicates structural absence, not a fix.

Pathology	LoRA	Proposed fix	GPart
$GL(r)$ non-uniqueness	\checkmark	ARROW, SpectR	\times
Scale non-invariance	\checkmark	ARROW, SpectR	\times
Coupled gradient dynamics	\checkmark	LoRA+, rsLoRA	\times
Initialization pathology	\checkmark	PiSSA, LoftQ	\times

The pattern is consistent: every identified pathology traces to either the representational non-uniqueness of the BA factorization or the asymmetric coupling of its two factors, and GPart eliminates both simultaneously by replacing the bilinear map with a single linear projection. This is not merely a list of engineering improvements; it is a structural consequence of recovering the clean theoretical properties that motivated the original intrinsic dimensionality hypothesis of Aghajanyan et al. [2021] before the BA detour was introduced.

G Licenses and asset usage

We document the external models and datasets used in this work, together with their source URLs and publicly stated licenses.

Natural language understanding. We use RoBERTa-base and RoBERTa-large, released by Facebook AI under the MIT License and available at <https://huggingface.co/roberta-base> and <https://huggingface.co/roberta-large>. We evaluate on the GLUE benchmark, available at <https://gluebenchmark.com/>; GLUE is a collection of public benchmark tasks whose component datasets are distributed under their respective licenses.

Mathematical reasoning. We use Qwen2.5-0.5B, Qwen2.5-3B, and Qwen2.5-7B from Qwen, available at <https://huggingface.co/Qwen/Qwen2.5-0.5B>, <https://huggingface.co/Qwen/Qwen2.5-3B>, and <https://huggingface.co/Qwen/Qwen2.5-7B>, released under Apache 2.0 license. We also use Gemma-7B, which is gated under Google’s Gemma usage license at <https://huggingface.co/google/gemma-7b>, and Llama-3.1-8B, which is distributed under the Llama 3.1 Community License at <https://huggingface.co/meta-llama/Llama-3.1-8B>. For training and evaluation, we use MetaMathQA (<https://huggingface.co/datasets/meta-math/MetaMathQA>), GSM8K (<https://huggingface.co/datasets/openai/gsm8k>), and MATH (<https://github.com/hendrycks/math>); these assets are commonly distributed under permissive academic/open licenses, with MetaMathQA and GSM8K publicly listed under MIT in prior work.

Vision. We use the Vision Transformer models ViT-Base and ViT-Large from Google, available at <https://huggingface.co/google/vit-base-patch16-224> and <https://huggingface.co/google/vit-large-patch16-224> and listed under the Apache 2.0 license. We evaluate on Oxford-IIIT Pets (<https://www.robots.ox.ac.uk/~vgg/data/pets/>), Stanford Cars (https://ai.stanford.edu/~jkrause/cars/car_dataset.html), CIFAR-10 (<https://www.cs.toronto.edu/~kriz/cifar.html>), DTD (<https://www.robots.ox.ac.uk/~vgg/data/dtd/>), EuroSAT (<https://github.com/phelber/EuroSAT>), FGVC-Aircraft (<https://www.robots.ox.ac.uk/~vgg/data/fgvc-aircraft/>), RESISC45 (<https://huggingface.co/datasets/timm/resisc45>), and CIFAR-100 (<https://www.cs.toronto.edu/~kriz/cifar.html>).

All assets were used in accordance with their publicly stated terms. We did not use proprietary or closed-access datasets.